Front. Electr. Electron. Eng. China (2006) 3: 355–360
DOI 10.1007/s11460-006-0046-8

RESEARCH ARTICLE

HUANG Ping-lin, HU Qian-sheng, YU Li, HUANG Yun-kai

Analysis of armature reaction and winding inductances of permanent magnet brushless DC motor with deep slot concentrated coils

Abstract Based on the configuration of deep slot concentrated coils, an analytical model is developed for predicting the armature reaction field produced by the 3-phase stator windings of permanent magnet brushless DC motors with concentrated coils by using the image method and the analytical functions of the armature reaction and winding inductances are proposed accounting for the influence of stator slotting. This approach is different from the method of equivalent distributed current sheet and more suitable for electric machines, which have concentrated coils and deeper slots. Under different control mode, the different analytical functions are presented. This will be helpful when further analyzing the performance of the motor. The results agree with the experiment very well.

Keywords the method of image, armature reaction, permanent magnet, deep slot concentrated coils, electric machinery

1 Introduction

The armature reaction field calculation in a brushless permanent magnet DC motor is important for the prediction of the dynamic performance of motors such as the radial exciting forces, the emitted acoustic noise, the demagnetization tolerance capability, and the self-and mutual-winding inductances [1–3]. In some papers the magnetic field distribution was obtained by a two-dimensional analytical technique [2], and the analytical model for predicting the armature reaction field was developed using the equivalent distributed current sheet [4–8]. For an electric machine that has shallow slots, this method is feasible since the error is not heavy.

However, some permanent magnet brushless DC motors with concentrated coils have deeper slots (shown in Fig. 1) to meet the requirements of force density, which differs from motors with overlapping or non-overlapping windings. It makes the method of equivalent distributed current sheet unsuitable due to the distribution of the coils in deep slots. Since the concentrated coils and deeper slots have been widely used in electric machines because of the simple form and manufacture convenience, it is important to calculate the armature reaction field of these machines accurately. The objective of this paper is to propose a new method to predict the armature reaction of permanent magnet brushless DC motors with concentrated coils and deep slots.

Concerning the configuration of these machines, this paper develops a magnetic calculation model using the image method. Based on this model, a calculation method of the armature reaction is presented. This approach is different from the equivalent distributed current sheet method and more suitable for electrical machines, which have concentrated coils and deeper slots. Besides these, the results under different control modes have been studied.

The purpose of this paper is to analyze the armature reaction of the permanent magnet brushless DC motor with concentrated coils and deeper slots. The analytical functions of the armature reaction under different control mode, as well as the graphs of field distribution are presented. Finally the predicted armature reaction and winding inductances for an experimental motor are deduced.

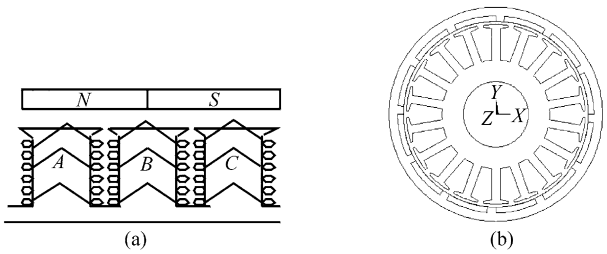

Fig. 1 Configuration of PMBLDCM with concentrated coils. (a) Deep slot concentrated coils; (b) Cross section of the brushless DC motor

Translated from *Proceedings of the Chinese Society for Electrical Engineering*, 2005, 25(12): 127–132 (in Chinese)

HUANG Ping-lin (✉), HU Qian-sheng, YU Li, HUANG Yun-kai
Department of Electronic Engineering, Southeast University, Nanjing 210096, China
E-mail: huangluo@ujs.edu.cn

2 The method of image

Based on the principle of the image method, while the permeability of the stator core and air-gap are concerned, the effect of the boundary could be represented by a visual image current, and the calculation current is $i' = (\mu_2 - \mu_1)i / (\mu_2 + \mu_1)$. Thus, the general solution of the vector magnetism in different regions is [9]:

$$\begin{cases} A_{z_1} = -\dfrac{\mu_1 i}{4\pi}\{\ln[x^2 + (y-h)^2] + \dfrac{\mu_2 - \mu_1}{\mu_2 + \mu_1}\ln[x^2 + (y-h)^2]\}, \\ y > 0 \\ A_{z_2} = -\dfrac{\mu_2 i}{4\pi}\left(\dfrac{2\mu_1}{\mu_1 + \mu_2}\right)\ln[x^2 + (y-h)^2],\ y < 0 \end{cases} \tag{1}$$

where $y > 0$ represents the region of air-gap, and $y<0$ represents the region of stator core, and

$$\begin{cases} B_x = \dfrac{\partial A}{\partial x} \\ B_y = \dfrac{\partial A}{\partial y} \end{cases} \tag{2}$$

For the permanent magnet brushless DC motor with concentrated coils, in order to simplify the calculation, two assumptions are given:

1) Neglect the influence of stator slot opening, and the permeability of the stator core is assumed to be uniform as μ_2.

2) Neglect the effect of the cross-section of the coils, and the length of the coils are assumed to be infinite, and the current through the coils is line current.

So the model of calculating the magnetic field is developed using the image method, shown in Fig. 2.

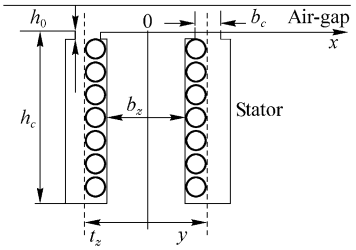

Fig. 2 Armature reaction calculation model for single tooth

Noticed that where

b_c is the width of the slots;

b_z is the width of the teeth;

h_c is the depth of the slot;

t_z is the interval of midlines of two slots;

h_0 is the height of the slots opening.

Since $h_0 << h_c$, it is neglected in this paper. For simplicity reasons, before computing the field of the concentrated coils, the field of the single coil is derived first according to Eq. (1).

$$A_{z_i} = -\frac{\mu_0 i}{4\pi}\left(\frac{2\mu_2}{\mu_2 + \mu_0}\right)\left\{\ln\left[\left(x - \frac{t_z}{2}\right)^2 + \left(y - \frac{kh_c}{N}\right)^2\right] - \ln\left[\left(x + \frac{t_z}{2}\right)^2 + \left(y - \frac{kh_c}{N}\right)^2\right]\right\} \tag{3}$$

where N is the number of the coils on one tooth. Then, the magnetic field produced by N coils is:

$$A_y = -\frac{\mu_0 i}{4\pi}\left(\frac{2\mu_2}{\mu_2 + \mu_0}\right)\sum_{k=1}^{N}\left\{\ln\left[\left(x - \frac{t_z}{2}\right)^2 + \left(y - \frac{kh_c}{N}\right)^2\right] - \ln\left[\left(x + \frac{t_z}{2}\right)^2 + \left(y - \frac{kh_c}{N}\right)^2\right]\right\}, \qquad y<0 \tag{4}$$

So, from Eq. (2) and Eq. (4) the radial flux density in air-gap produced by winding on single tooth is

$$B_{\delta y}(x, y) = -\frac{\mu_0 i}{4\pi}\left(\frac{2\mu_2}{\mu_2 + \mu_0}\right) \cdot \sum_{k=1}^{N}\left\{\frac{2\left(x - \frac{t_z}{2}\right)}{\left(x - \frac{t_z}{2}\right)^2 + \left(y - \frac{kh_c}{N}\right)^2} - \frac{2\left(x + \frac{t_z}{2}\right)}{\left(x + \frac{t_z}{2}\right)^2 + \left(y - \frac{kh_c}{N}\right)^2}\right\}, \quad y < 0 \tag{5}$$

In Eq. (5), when k equals an appointed integer ranging from 1 to N, we can calculate the magnetic field produced by the kth single coil. When N =10, and k equals to 1, 5 and 10, respectively, they are shown in Fig. 3. For comparison, the field produced by single coil is calculated according to the paper [2], and it is shown in Fig. 3(d). Obviously, the value calculated by the latter approach is greater than the former because the latter based on the theory of equivalent distributed current sheet. When the slot depth is smaller, the

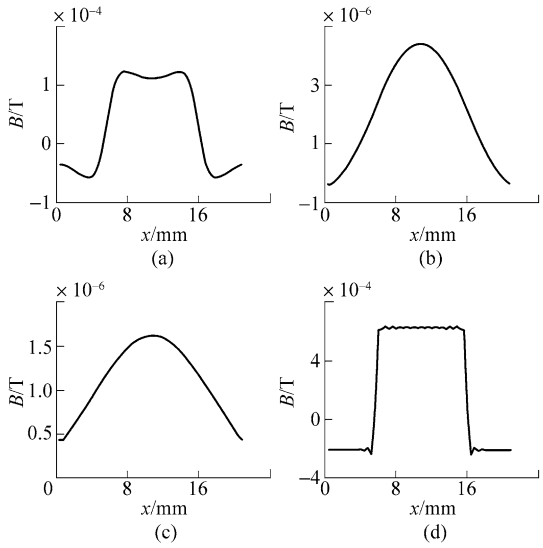

Fig. 3 Air-gap magnetic field produced by single coil. (a) k=1; (b) k=5; (c) k=10; (d) The single coil at the stator surface

influence of the depth of slots is not significant, and the results obtained using the method of equivalent distributed current sheet are acceptable. The curve in Fig. 3(a) shows the results of the single coil at topside in slot, which is close to, but still below, the surface of the stator. The curve in Fig. 3(d) shows the results when the single coil is just at the surface of the stator. Although they look different, they approach each other. But with increasing the slot depth, it tends to deviate significantly such as shown in Fig. 3(b) and Fig. 3(c). It is evident that the method of equivalent distributed current sheet is unsuitable when the stator has deep slots.

3 Armature reaction field of 3-phase windings

In Sect. 2 the magnetic field produced by single coil and winding was analyzed, and the analytical function was deduced as Eq. (5). For the 3-phase machine, when operating while not all of the phases have current in the same way, each phase has a respective rule corresponding to the control model such as six-step control and three-step control model. Thus, a different control mode will result in different armature reaction field. So, the objective of this section is to investigate the armature reaction field of 3-phase windings under different control models.

By calculating, when $i=1\text{A}$, the distribution graph of the experimental motor produced by winding on single tooth is shown in Fig. 4.

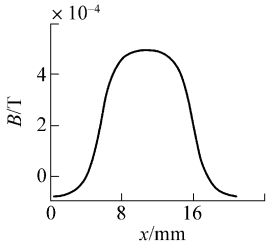

Fig. 4 Magnetic field produced by winding on single tooth

Hence the radial field produced by one phase concentrated winding in a brushless DC motor can be deduced from Eq. (5) as:

$$B_{\delta y}(x,y)=-\frac{\mu_0 i}{4\pi}\left(\frac{2\mu_0 b_c+2\mu_{\text{Fe}}b_z}{2\mu_0 b_c+(\mu_{\text{Fe}}+\mu_0)b_z}\right)\cdot\sum_{n=0}^{q/m-1}\sum_{k=1}^{N}\left\{\frac{2\left(x-\frac{t_Z}{2}+nmt_z\right)}{\left(x-\frac{t_z}{2}+nmt_z\right)^2+\left(y-\frac{kh_c}{N}\right)^2}-\frac{2\left(x+\frac{t_z}{2}+nmt_z\right)}{\left(x+\frac{t_z}{2}+nmt_z\right)^2+\left(y-\frac{kh_c}{N}\right)^2}\right\},\quad y<0 \tag{6}$$

where m is the number of the phase, and q is the number of the slots.

For the 3-phase brushless DC motor, under different control modes, the number of phases with current pass through is different. For the three-step mode, there is always only one phase carrying a current, while for the six-step control model, there are always two phases carrying a current. Then, the armature reaction field is distinct when the control mode is changed.

For the three-step control mode, it has the similar state as a one-phase winding. So the armature reaction function is Eq. (6), and the graph is shown in Fig. 5.

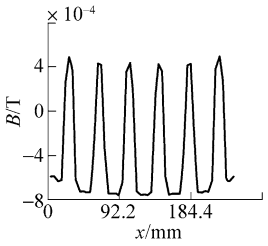

Fig. 5 Magnetic field along rotor circumference of three-step control

Further, from Eq. (5) we can deduce the armature reaction analytical function when six-step control is used in Eq. (7), and the graph is shown in Fig. 6.

$$B_{\delta y}(x,y)=-\frac{\mu_0 i}{4\pi}\left(\frac{2\mu_0 b_c+2\mu_{\text{Fe}}b_z}{2\mu_0 b_c+(\mu_{\text{Fe}}+\mu_0)b_z}\right)\cdot\sum_{n=0}^{q/m-1}\sum_{k=1}^{N}\left\{\frac{2\left(x-\frac{t_z}{2}+nmt_z\right)}{\left(x-\frac{t_z}{2}+nmt_z\right)^2+\left(y-\frac{kh_c}{N}\right)^2}-\frac{4\left(x+\frac{t_z}{2}+nmt_z\right)}{\left(x+\frac{t_z}{2}+nmt_z\right)^2+\left(y-\frac{kh_c}{N}\right)^2}+\frac{2\left(x+\frac{3t_z}{2}+nmt_z\right)}{\left(x+\frac{3t_z}{2}+nmt_z\right)^2+\left(y-\frac{kh_c}{N}\right)^2}\right\} \tag{7}$$

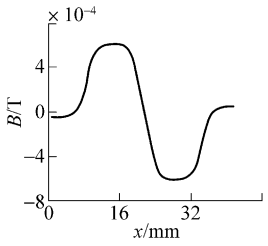

Fig. 6 Magnetic field under a pair of poles of six-step control

4 Winding inductances

Similarly, by using the image method, the magnetic field in the teeth produced by the kth single coil is obtained from Eq. (8)

$$B_k(x,y) = -\frac{\mu_2 i}{2\pi}\left\{\frac{x-\frac{b_z}{2}}{\left(x-\frac{b_z}{2}\right)^2+\left(y-\frac{kh_c}{N}\right)^2} - \frac{x+\frac{b_z}{2}}{\left(x+\frac{b_z}{2}\right)^2+\left(y-\frac{kh_c}{N}\right)^2}\right\} - \frac{\mu_2 i}{2\pi}\frac{\mu_0-\mu_2}{\mu_0+\mu_2}\left\{\frac{x-\frac{b_z}{2}}{\left(x-\frac{b_z}{2}\right)^2+\left(y+\frac{kh_c}{N}\right)^2} - \frac{x-\frac{b_z}{2}}{\left(x+\frac{b_z}{2}\right)^2+\left(y+\frac{kh_c}{N}\right)^2}\right\}, \quad k=1,2,\cdots,N \tag{8}$$

Considering the symmetry of the armature, for one single tooth, the magnetic field distribution can be described as Eq. (9).

$$B_{ty}(x,y) = -\frac{\mu_2 i}{2\pi}\sum_{k=1}^{N}\left\{\frac{x-\frac{b_z}{2}}{\left(x-\frac{b_z}{2}\right)^2+\left(y-\frac{kh_c}{N}\right)^2} - \frac{x+\frac{b_z}{2}}{\left(x+\frac{b_z}{2}\right)^2+\left(y-\frac{kh_c}{N}\right)^2}\right\} - \frac{\mu_2 i}{2\pi}\frac{\mu_0-\mu_2}{\mu_0+\mu_2}\sum_{k=1}^{N}\left\{\frac{x-\frac{b_z}{2}}{\left(x-\frac{b_z}{2}\right)^2+\left(y+\frac{kh_c}{N}\right)^2} - \frac{x+\frac{b_z}{2}}{\left(x+\frac{b_z}{2}\right)^2+\left(y+\frac{kh_c}{N}\right)^2}\right\}, \quad -\frac{b_z}{2}\le x\le\frac{b_z}{2},\quad 0\le y\le h_c \tag{9}$$

So the flux of the kth coil is:

$$\phi_k = B_{ty}(0,\frac{kh_c}{N})b_Z l \tag{10}$$

where l is the axial length of the motor. The flux produced by coils on one tooth is:

$$\begin{aligned}\phi &= b_z l\sum_{v=1}^{N}B_{ty}\left(0,\frac{vh_c}{N}\right)\\ &= b_z l\sum_{v=1}^{N}\left(-\frac{\mu_2 i}{2\pi}\cdot\sum_{k=1}^{N}\left\{\frac{-\frac{b_z}{2}}{\left(-\frac{b_z}{2}\right)^2+\left(\frac{vh_c}{N}-\frac{kh_c}{N}\right)^2} - \frac{x+\frac{b_z}{2}}{\left(\frac{b_z}{2}\right)^2+\left(\frac{vh_c}{N}-\frac{kh_c}{N}\right)^2}\right\}\right.\\ &\quad -\frac{\mu_2 i}{2\pi}\frac{\mu_0-\mu_2}{\mu_0+\mu_2}\sum_{k=1}^{N}\left\{\frac{-\frac{b_z}{2}}{\left(-\frac{b_z}{2}\right)^2+\left(\frac{vh_c}{N}+\frac{kh_c}{N}\right)^2}\right.\\ &\quad \left.\left.-\frac{\frac{b_z}{2}}{\left(\frac{b_z}{2}\right)^2+\left(\frac{vh_c}{N}+\frac{kh_c}{N}\right)^2}\right\}\right)\end{aligned} \tag{11}$$

and the flux linkage of one phase is

$$\varphi_m = \frac{\phi Q_s}{m} \tag{12}$$

where Q_s is the number of the stator tooth; m is the number of phase.

Hence the inductance of one phase is:

$$L_\phi = \frac{\varphi_m}{a_i} \tag{13}$$

where a is the number of parallel circuits.

5 Experimental result and analysis

One twelve-pole, three-phase external rotor experimental permanent magnet machine has been considered. Inductances of single coil in different slot positions obtained by analytical method, FEM method and measuring are listed in Table 1. The table shows that the analytical method is consistent with the FEM method and the measuring result. The magnetic field distribution in the tooth is shown in Fig. 7.

For the experimental machine, the computed phase inductance is 24.89 mH, and the measured one is 25.31 mH. The error is less than 2%.

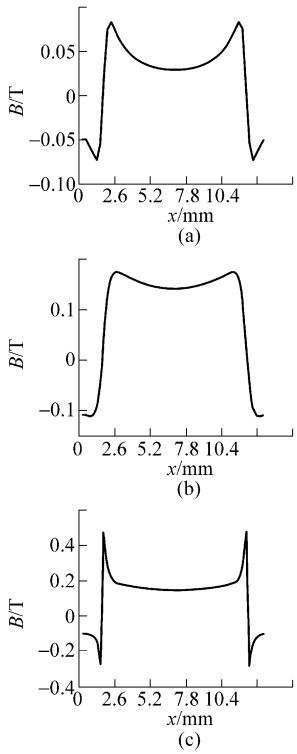

Fig. 7 Magnetic field distribution in tooth. (a) y =1 mm; (b) y =7 mm; (c) y =15.4 mm

From Table 1 and Fig. 7, we can see that for deep slots the inductances of single coil in different slot positions are different and the magnetic field distribution in the tooth varies with the height.

Table 1 Inductances of single coil in different slot position

k	Computed/μH	Measured/μH	FEM/μH	Error/%
1	0.362	0.372	0.375	2.69
5	0.438	0.420	0.432	4.30
10	0.513	0.490	0.515	4.70

Allowing for the armature reaction and the influence of the phase inductance, the simulated phase current waveform of the experimental machine at rated speed is shown in Fig. 8(a), and the measured one is shown in Fig. 8(b). They match very well.

6 Conclusions

Based on the configuration of deep slot concentrated coils, a new analytical model is developed for predicting the armature reaction field produced by the 3-phase stator windings of permanent magnet brushless DC motors with concentrated coils by using the image method. It is important to notice that under different control modes the analytical functions are different. By comparison with the FEM method and experiment, this method is more precise, especially when the stator has deep slots. Besides this, the analytical function of the winding inductances is proposed accounting for the influence of deep slots. Experimental results show that the proposed method is valid.

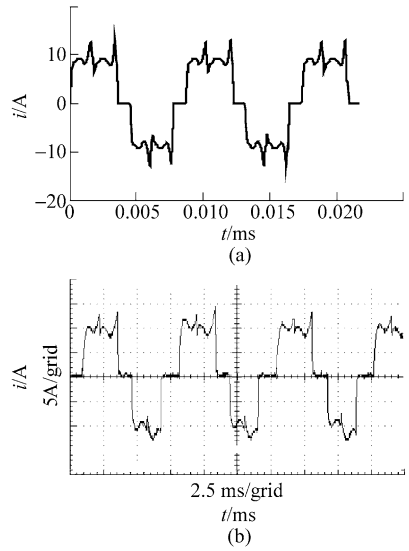

Fig. 8 Phase current waveform. (a) Computed; (b) Measured

Table 2 The parameters of the experimental motor

	mm
Stator exterior diameter	88
Rotor interior diameter	91
Slot number of stator	18
Width of the slots	3
Depth of the slot	15.4
Interval of midlines of two slots	15.4
Width of the teeth	12.4
Conductor number in per slot of one phase	10
Length of the armature	30

References

1. Howe D., Zhu Z. Q., Chan C. C. et al., Improved analytical model for predicting the magnetic field distribution in brushless permanent–magnet machines, IEEE Transactions on Magnetics., 2002, 38(1): 229–238
2. Zhu Z. Q., Howe D., Instantaneous magnetic field distribution in brushless permanent magnet DC motors，part Ⅱ: armature – reaction field, IEEE Transactions on Magnetics., 1993, 29(1)：136–142
3. Li Kun-peng., Hu Qian-sheng., Huang Yun-kai , The circuit model of the permanent magnet brushless DC motor allowing for its windings inductances and its analysis, Proceedings of the Chinese Society for Electrical Engineering, 2004，24(1): 77–80 (in Chinese)
4. Miller T. E., Calculation of inductance in permanent magnet

DC motors, IEE Proc-Electr. Power Appl., March 1999, 146(2): 129–137
5. Zhang H., Pan Z. P., Computation of permanent magnet brushless DC motor design allowing for inductance, 4th IEEE International Conference on Power Electronics and Drive Systems, Oct 22-25 2001, Denpasar, Bali, 2001(2): 815–818
6. Wang Xing-hua., Li Qing-fu, Wang Shu-hong, et al, Analytical calculation of no-load air-gap magnetic field and back electromotive force in brushless DC motor, Proceedings of the Chinese Society for Electrical Engineering, 2003, 23(3): 126–130 (in Chinese)
7. Shimasaki T., Tateishi S., Small and lightweight cleaner motor, National Technical Report., 40(5): 49–54
8. Zhu Z. Q., Howe D., Instantaneous magnetic field distribution in brushless permanent magnet DC motor, IEEE transactions on magnetics, January 1993, 29(1): 136–142
9. Tang Yun-miu, The magnetic field in electric machine, Beijing: Science Press, 1981 (in Chinese)